



## Research article

# Transcriptomic analysis reveals Cilostazol's role in ameliorating cardiovascular disease: Inhibition of monocyte-to-macrophage differentiation and reduction of endothelial cell reactive oxygen species production

Chia-Ning Fan <sup>a,b,1</sup>, Tsung-Neng Tsai <sup>c,1</sup>, Xin-Jie Lu <sup>d</sup>, Hsing-Fan Lai <sup>d,e</sup>,  
Chun-Hua Wang <sup>d</sup>, Yi-Lin Chiu <sup>d,\*</sup>

<sup>a</sup> Department of Surgery, Taoyuan Armed Forces General Hospital, Taoyuan, 325, Taiwan (R.O.C.)

<sup>b</sup> Division of Cardiovascular Surgery, Department of Surgery, Tri-Service General Hospital, National Defense Medical Center, Taipei, 114, Taiwan (R.O.C.)

<sup>c</sup> Division of Cardiology, Department of Internal Medicine, Tri-Service General Hospital, National Defense Medical Center, Taipei, 114, Taiwan (R.O.C.)

<sup>d</sup> Department of Biochemistry, National Defense Medical Center, Taipei, 114, Taiwan (R.O.C.)

<sup>e</sup> Graduate Institute of Life Sciences, National Defense Medical Center, Taipei city, 114, Taiwan (R.O.C.)

## A B S T R A C T

**Background:** Cardiovascular diseases (CVDs) are the leading global cause of death, with atherosclerosis as the primary cause. Chronic inflammation, endothelial dysfunction, and the role of molecules like nitric oxide and reactive oxygen species are crucial in this context. Our previous research indicated that cilostazol and ginkgo biloba extract could enhance the ability of endothelial cells to dissolve blood clots, but the effects of cilostazol on monocytes remain unexplored.

**Method:** This study utilized peripheral blood mononuclear cells from 10 healthy donors, treated ex vivo with cilostazol. RNA-sequencing, over-representation analysis, xCell stromal cell analysis, and Gene Set Enrichment Analysis were employed to investigate the gene expression changes and biological pathways affected by cilostazol treatment.

**Results:** The study identified specific gene sets and pathways that were enriched or reduced in response to cilostazol treatment, providing insights into its effects on monocytes and potential therapeutic applications in CVD. The analysis also revealed the potential impact of cilostazol on the stromal cell compartment, further broadening our understanding of its multifaceted role.

**Conclusion:** The findings offer a nuanced understanding of the advantages and mechanisms of cilostazol in CVD, uncovering novel therapeutic targets and strategies to enhance the clinical application of cilostazol and contributing to the broader implications of this therapy in cardiovascular health.

## 1. Introduction

Cardiovascular diseases (CVDs) are the leading cause of death globally, significantly contributing to health loss and high healthcare system costs [1]. Atherosclerosis, characterized by arterial plaque buildup, is the primary cause of CVD. Chronic inflammation, linked with endothelial cell dysfunction, appears to govern the disease process [2,3], necessitating clinical research into anti-inflammatory and immunomodulatory treatments. Inflammation is a key factor in atherosclerosis and CVD. The roles of immune-active cells,

\* Corresponding author.

E-mail address: [yilin1107@mail.ndmctsgh.edu.tw](mailto:yilin1107@mail.ndmctsgh.edu.tw) (Y.-L. Chiu).

<sup>1</sup> These authors contributed equally to the work.

<https://doi.org/10.1016/j.heliyon.2024.e29194>

Received 27 August 2023; Received in revised form 1 April 2024; Accepted 2 April 2024

Available online 3 April 2024

2405-8440/© 2024 Published by Elsevier Ltd.

This is an open access article under the CC BY-NC-ND license

(<http://creativecommons.org/licenses/by-nc-nd/4.0/>).

pro-inflammatory cytokines, chemokines, and lipid mediators are crucial in this context [4]. Dead cells and the oxidized forms of low-density lipoprotein are particularly abundant in atherosclerosis [5]. Oxidized low-density lipoprotein, known for its immunogenic properties, can activate endothelial cells, leading to monocyte adhesion and differentiation into macrophages [6,7]. Within atherosclerotic plaques, macrophages tend to accumulate and exhibit reduced migratory ability, leading to unresolved inflammation and progression to more complex plaques [8,9]. Macrophages contribute to inflammation by secreting pro-inflammatory mediators and matrix-degrading proteinases. Dying macrophages release lipid components and tissue factors, forming a prothrombotic necrotic core, a key component of unstable plaques that can rupture.

The “Response-to-Injury Hypothesis” by Ross and Glomset outlines the potential process from endothelial dysfunction to atherosclerosis [10]. This hypothesis has been instrumental in understanding the underlying mechanisms that lead to atherosclerotic plaque development. A key characteristic of endothelial dysfunction is the loss of nitric oxide (NO) bioactivity [3], a critical molecule involved in vascular homeostasis. NO plays a vital role in maintaining vascular tone, inhibiting platelet aggregation, and preventing the adhesion of monocytes to the endothelium. The loss of NO bioactivity can lead to a cascade of events contributing to atherosclerosis. One of the factors closely related to NO production is the generation of reactive oxygen species (ROS). ROS are molecules that play a dual role in the vascular system. On one hand, elevated ROS levels are associated with reduced NO bioavailability [11]. This reduction in NO bioavailability can lead to vasoconstriction, increased platelet aggregation, and enhanced adhesion of monocytes to the endothelium, which are key events in the initiation of atherosclerosis. ROS may also cause an increase in monocyte-endothelium adhesion [12], promoting the inflammatory response that characterizes atherosclerosis. On the other hand, ROS are essential for macrophage differentiation [13], a process central to the immune response and atherosclerotic plaque progression. Macrophages are key players in the inflammatory response, and their differentiation and function are tightly regulated by various signaling pathways, including those involving ROS.

Cilostazol, characterized by its antithrombotic, vasodilatory, antimitogenic, and cardiogenic properties, has been broadly investigated because of its multifaceted efficacy in CVD management [14]. Its application in CVD is substantiated by its demonstrated superiority over clopidogrel in reducing the incidence of recurrent ischemic strokes in those with non-cardioembolic ischemic stroke [15]. Furthermore, the combination of cilostazol and aspirin is comparable or superior to that of aspirin and clopidogrel in preventing stent restenosis [16]. Regarding cardiovascular event prevention, cilostazol has been associated with a notably low rate of serious events, including myocardial infarction, observed in only 1% of the patients treated with cilostazol [17]. Lin et al. further elucidated the drug’s efficacy in significantly reducing the risk of major coronary events, major adverse cardiovascular and cerebrovascular events, and symptoms of angina pectoris [18]. The influence of cilostazol on circulating endothelial progenitor cell counts, which are pivotal markers in cardiovascular health, also surpasses that of aspirin, suggesting an additional therapeutic benefit [19]. Moreover, combining cilostazol with aspirin may mitigate biological resistance to aspirin in ischemic stroke [20]. Crucially, cilostazol significantly reduces the risk of cerebrovascular events in patients with atherothrombosis, without a corresponding increase in bleeding risk, thereby offering a safety advantage over other antiplatelet agents [21]. This safety profile is particularly relevant for patients with a history of hypertension or gastrointestinal bleeding, where cilostazol may be a safer alternative than clopidogrel [22].

Our previous research focusing on endothelial cells discovered that both cilostazol and ginkgo biloba extract could enhance the expressions of endothelial cell thrombomodulin (TM) and endothelial NO synthase (eNOS) by activating the Krüppel-like factor 2 (KLF2) axis. This activation subsequently increased the endothelial cells’ ability to dissolve blood clots [23–25]. These findings provide valuable insights into the potential therapeutic applications of cilostazol and ginkgo biloba extract in cardiovascular health. However, the literature has not explored whether cilostazol has any other effects on monocytes. This knowledge gap prompted our current study, aiming to shed light on the broader implications of cilostazol in CVD and to enhance the precision of its clinical application. In this study, we utilized peripheral blood mononuclear cells (PBMC) from healthy donors and treated them *ex vivo* with cilostazol. We comprehensively analyzed the gene expression changes induced by cilostazol treatment through RNA sequencing. Over-representation analysis was employed to identify the biological pathways significantly affected by the treatment. Additionally, we utilized xCell immune and stromal cell analysis to investigate the potential impact of cilostazol on the stromal cell compartment. Gene Set Enrichment Analysis (GSEA) further allowed us to identify specific gene sets and pathways that were enriched or depleted in response to cilostazol treatment. The findings from this study are expected to provide a more nuanced understanding of the advantages and mechanisms of cilostazol in the context of CVD. By exploring the effects of cilostazol on monocytes, we hope to uncover novel therapeutic targets and strategies that could enhance the efficacy and precision of cilostazol in clinical settings.

## 2. Material and methods

### 2.1. IRB approval and PBMC treatment

This study was conducted with the approval of the institutional review boards at both the Tri-Service General Hospital and the Taipei Veteran General Hospital, under IRB number 2012-03-001AC. In accordance with the ethical guidelines set forth in the 1975 Helsinki Declaration, all participants in this study provided their written informed consent. Furthermore, all experimental procedures and protocols involving animals were not only approved by the Institutional Animal Care and Use Committee (IACUC) of National Yang-Ming University but were also in full compliance with the ARRIVE guidelines.

Ten healthy donors were recruited for the study, and blood samples were obtained. PBMC were isolated from the blood samples using Ficoll-Paque Plus (Sigma-Aldrich, Inc., St. Louis, MO, USA, Cat.: GE17-1440-02) in Leucosep™ tubes (Greiner Bio-One, Krefeld, Germany), according to the manufacturer’s instructions. Following isolation, the PBMC were cultured in RPMI 1640 medium, supplemented with 10% Fetal Bovine Serum (FBS, Thermo-Fisher Scientific Inc., Waltham, MA, USA) and 1% penicillin/

streptomycin. The cells were treated with 30  $\mu$ M cilostazol and an appropriate vehicle control and were incubated for 24 h at standard culture conditions.

## 2.2. RNA sequencing and differentially expressed genes (DEG) analysis

Treated PBMCs were subjected to RNA extraction and analysis via next-generation sequencing. The extraction process was facilitated by the use of TRIzol Reagent (Thermo-Fisher Scientific). Following extraction, the RNA samples were quantified and analyzed through the NanoDrop device (Thermo-Fisher Scientific), as well as the Agilent 2100 Bioanalyzer system (Agilent Technologies). The visualization and integrity of the RNA were evaluated using 1% agarose gel electrophoresis. Subsequently, we purified the mRNA using both Poly(A) mRNA Bead Isolation Kits and rRNA Removal Kits. First-strand cDNA synthesis was accomplished using ProtoScript II Reverse Transcriptase following mRNA fragmentation with First Strand Synthesis Reaction Buffer and Random Primer. We then synthesized Second Strand DNA by leveraging the Second Strand Synthesis Enzyme Mix. DNA fragments were then polished using End Prep Enzyme Mix. Adaptors were attached to both ends of the fragments via a process of dA-tailing and T-A ligation. A 420bp fraction of fragments was subsequently isolated through the application of magnetic beads. A 13-cycle PCR was then performed using P5 and P7 primers. The resulting library was quantified with a Qubit 3.0 fluorometer and sequenced on an Illumina HiSeq 4000 platform. The resulting sequencing data in fastq format was processed and generated by GENEWIZ®. Transcript abundance for each sample was estimated by separately running two iterations using both Salmon (v0.91) and Kallisto (v0.46.2) in combination with the GRCh38 human reference transcript from GENCODE v41 [26]. These tools quasi-mapped the sequencing reads using a 31bp k-mer index. Subsequently, a third iteration was conducted using Salmon (v0.91) in combination with the human reference transcript downloaded from Ensembl (Homo\_sapiens.GRCh38.cdna.all.fa.gz) [27]. The tximport package (v1.24.0) facilitated the importation of transcript abundance estimates from the files generated by Salmon and Kallisto for analysis in the R (v4.2.2) statistical programming environment. Transcript abundance estimates were then aggregated into gene expression counts at the gene level. The resultant raw counts were merged for use in downstream analyses. DEGs for cilostazol treatment were identified using the EdgeR package (v3.40.2). Criteria for selection of differentially expressed genes:  $|\log_2 \text{fold change}| \geq 1$ ; Benjamini-Hochberg (B-H) adjusted P-value  $< 0.05$ .

## 2.3. Over representative analysis and visualization

Details on differentially expressed genes (DEGs) are provided in the supplementary table. To interpret the potential biological implications of these DEGs, over-representation analysis (ORA) was carried out to uncover significantly enriched biological processes, molecular functions, and cellular components. The DEGs were categorized into three clusters based on stringent criteria: Cluster “>1” with an absolute  $\log_2$  fold change greater than 1 and FDR less than 0.05, resulting in 546 up-regulated and 631 down-regulated genes. Cluster “>2” with an absolute  $\log_2$  fold change greater than 2 and FDR less than 0.05, resulting in 129 up-regulated and 125 down-regulated genes. Cluster “>3” with an absolute  $\log_2$  fold change greater than 3 and FDR less than 0.05, resulting in 54 up-regulated and 32 down-regulated genes. Gene Ontology (GO) enrichment analysis for biological processes (BP), molecular functions (MF), and cellular components (CC) was performed on these three clusters using the compareCluster function of the clusterProfiler package (v4.4.4) in R [28]. The fun was set to “enrichGO” with ontologies (ont) set as “BP”, “MF”, and “CC”, and the showCategory parameter set to 3. To streamline the representation of similar gene sets, the “simplify” function was utilized with a cutoff of 0.7 by adjusted p-value (by = “p.adjust”). Visualization of the enriched GO terms was performed using the “dotplot” function, with the dot size determined by the negative log of the FDR ( $-\log_{10} \text{FDR}$ ) and color indicating the gene ratio. For pathway enrichment analysis, a similar approach was adopted, but the “fun = enricher” was employed. The analysis incorporated KEGG\_2021\_Human (320 gene sets), WikiPathway\_2021\_Human (622 gene sets), and Reactome\_2022 (1818 gene sets) databases, which were downloaded from the EnrichR platform [29].

For the visualization of over-representation analysis (ORA), Cytoscape (v3.9.1) along with the ClueGo app was utilized, focusing on the 546 up-regulated and 631 down-regulated genes identified in our study [30,31]. The ClueGo app in Cytoscape was set up to reference multiple databases, including Gene Ontology biological processes (GOBP), Gene Ontology molecular functions (GOMF), Gene Ontology cellular components (GOCC), KEGG, Reactome, and WikiPathways with the default parameters.

## 2.4. Gene Expression Omnibus (GEO) database access

Public datasets were accessed from the National Center for Biotechnology Information’s Gene Expression Omnibus (NCBI GEO) database to validate our findings related to cardiovascular diseases. Dataset GSE19151 included 70 adults with prior venous thromboembolism (VTE) on warfarin and 63 healthy controls, analyzed using Affymetrix Human Genome U133A 2.0 Array ( $\log_2$  RMA signal) [32]. Dataset GSE28829 contained samples from atherosclerotic carotid artery segments, including 16 advanced and 13 early plaques, analyzed with Affymetrix Human Genome U133 Plus 2.0 Array (RMA-calculated signal intensity) [33]. Dataset GSE100927 comprised samples from 69 atherosclerotic and 35 control arteries from deceased organ donors, analyzed using Agilent-039494 SurePrint G3 Human GE v2  $8 \times 60\text{K}$  Microarray (normalized signal intensity  $\ln$ ) [34]. All datasets were obtained from publicly available GEO database repositories, and the corresponding microarray data and patient follow-up information were used for analysis, with raw data preprocessed and normalized as required for the specific microarray platforms, and appropriate statistical methods applied for validation of our findings.

### 3. Cell subsets enumeration using xCell approach

For a comprehensive understanding of the cellular composition of the samples, the xCell analysis was employed to enumerate various cell subsets in the gene expression data [35]. This analysis was carried out using the IOBR package (version 0.99.9) in R (v4.2.0), specifically employing the `deconvo_tme` function with the `method` parameter set to "xcell" and `arrays` set to "TRUE" [36]. The 64 cell types identified were categorized into five major classes: Lymphoid, Stem cells, Myeloids, Stromal Cells, and Others. This categorization allowed for an in-depth analysis of the cell subsets within the samples, enabling a nuanced understanding of their respective roles and interactions. A heatmap was constructed to visualize the hierarchical clustering of the data. Utilizing the Euclidean distance as the metric, the clustering was executed using the Morpheus web tool. The raw data were standardized using Z-score normalization to ensure comparability across the different samples. Statistical analysis was performed using a *t*-test to compare the samples to the control group. The results were visualized through violin plots, drawn using the `ggplot2` package (v3.4.2) in R.

#### 3.1. Machine learning algorithms

Supervised machine learning algorithms were employed to predict the relative scores of PBMCs being identified as diseased post cilostazol treatment. To predict the relative likelihood of PBMCs being classified as diseased following cilostazol treatment, we employed a series of supervised machine learning algorithms. Machine learning analysis was conducted using Orange (v3.35) [37]. The xCell signatures of each database were imported into Orange via the widget "CSV File Import" feature. For cross-validation, we used the widget "Data Sampler". We created 10 subsets and reserved 1 as an unused subset. We configured the widget "Neural Network" with 3,6,3 neurons in the hidden layers and employed ReLu as the activation function. The Adam method was selected as the solver and regularization was set to  $\alpha = 0.0001$ . The maximum number of iterations was set to 200, and replicable training was enabled. The "Random Forest" widget was configured with 500 trees. The option in Growth Control "Do not split subsets smaller than" was set to 5. For logistic regression, we utilized the widget "Logistic Regression". The regularization type was set to Ridge (L2), and strength was set at  $C = 1$ . Widget "Test and Score" was used for cross-validation with a number of folds set to 10. The "stratified" option was selected. ROC Analysis was carried out using the widget "ROC Analysis". The target was set to venous thromboembolism (VTE), advanced atherosclerotic plaque, and atherosclerotic artery, respectively. The widget "Prediction" was used to calculate the cardiovascular disease score for samples of PBMCs both with and without cilostazol treatment. The predicted scores were saved using the widget "Save Data" feature. The resulting data were then exported to R for visualization and statistical analysis using the `ggplot2` package (v3.4.2). Specifically, bar plots were created to illustrate the predictive scores of cardiovascular diseases for the different treatment groups.

#### 3.2. Gene Set Enrichment Analysis (GSEA)

GSEA was executed to discern gene sets that showed statistically significant, concordant differences between cilostazol-treated and untreated samples. The analysis was carried out using the `gseplot2` function within the `enrichplot` package (v1.16.2). The gene sets were derived from various sources, including the vascular endothelial cell activation pathway related to growth factor, NO, and ROS in triggering vascular inflammation from the Elsevier Pathway Collection; fibrin clot-associated gene sets from the Reactome pathway; regulation of ROS biosynthetic process and metabolic process from the Gene Ontology Biological Process (GOBP); macrophage behavior from the MGI Mammalian Phenotype Level 4 2021, filtered by "macrophage"; and macrophage biomarker gene sets from the CellMarker database, filtered by "macrophage" and "peripheral blood." All these gene sets are available for download from `enrichR` [29]. A Gene-Concept Network was constructed using the `cnplot` function in the `enrichplot` package (v1.16.2), and a heatmap-like plot for functional classification was created with the `heatmap` function in the same package.

#### 3.3. Cell viability assay and reactive oxygen species production assay

The production of ROS in Human Umbilical Vein Endothelial Cells (HUVEC) was assessed to gauge cellular oxidative stress status. Initially, cell viability was evaluated using the MTT assay (Sigma-Aldrich, Cat.: M5655), treating cells with vehicle (DMSO, Thermo-Fisher Scientific; Cat.: 036480.K2) and cilostazol at concentrations of 10  $\mu$ M, 30  $\mu$ M, and 100  $\mu$ M. After a 24-h incubation, optical density (OD) was measured to calculate relative cell viability. Subsequently, ROS production was quantified using the H2DCFDA (Thermo-Fisher Scientific; Cat.: D399) method. This fluorescent dye is oxidized by ROS into a highly fluorescent compound, allowing ROS detection within the cells using a BD FACSCanto™ II flow cytometry system (Becton, Dickinson and Company, Franklin Lakes, NJ, USA). Cells were seeded and allowed to adhere before treatment with cilostazol (0.1  $\mu$ M, 1  $\mu$ M, 10  $\mu$ M, and 30  $\mu$ M), then treated with H2DCFDA and incubated under specified conditions for ROS production. Following incubation, ROS levels were detected and quantified through flow cytometry.

#### 3.4. Flow cytometry detecting macrophage differentiation markers

Flow cytometry was employed to detect specific markers of macrophage differentiation, providing validation of the impact of cilostazol on monocyte differentiation into macrophages. The THP-1 acute monocytic leukemia cell line was cultured in RPMI1640 growth medium with 10% Fetal Bovine Serum (FBS, Thermo-Fisher Scientific) and treated with DMSO and cilostazol at a concentration of 30  $\mu$ M for 24 h. The specific markers CD80-APC (Elabscience Biotechnology Co., Ltd., Wuhan, Hubei, China, Cat.: E-AB-F1232E),

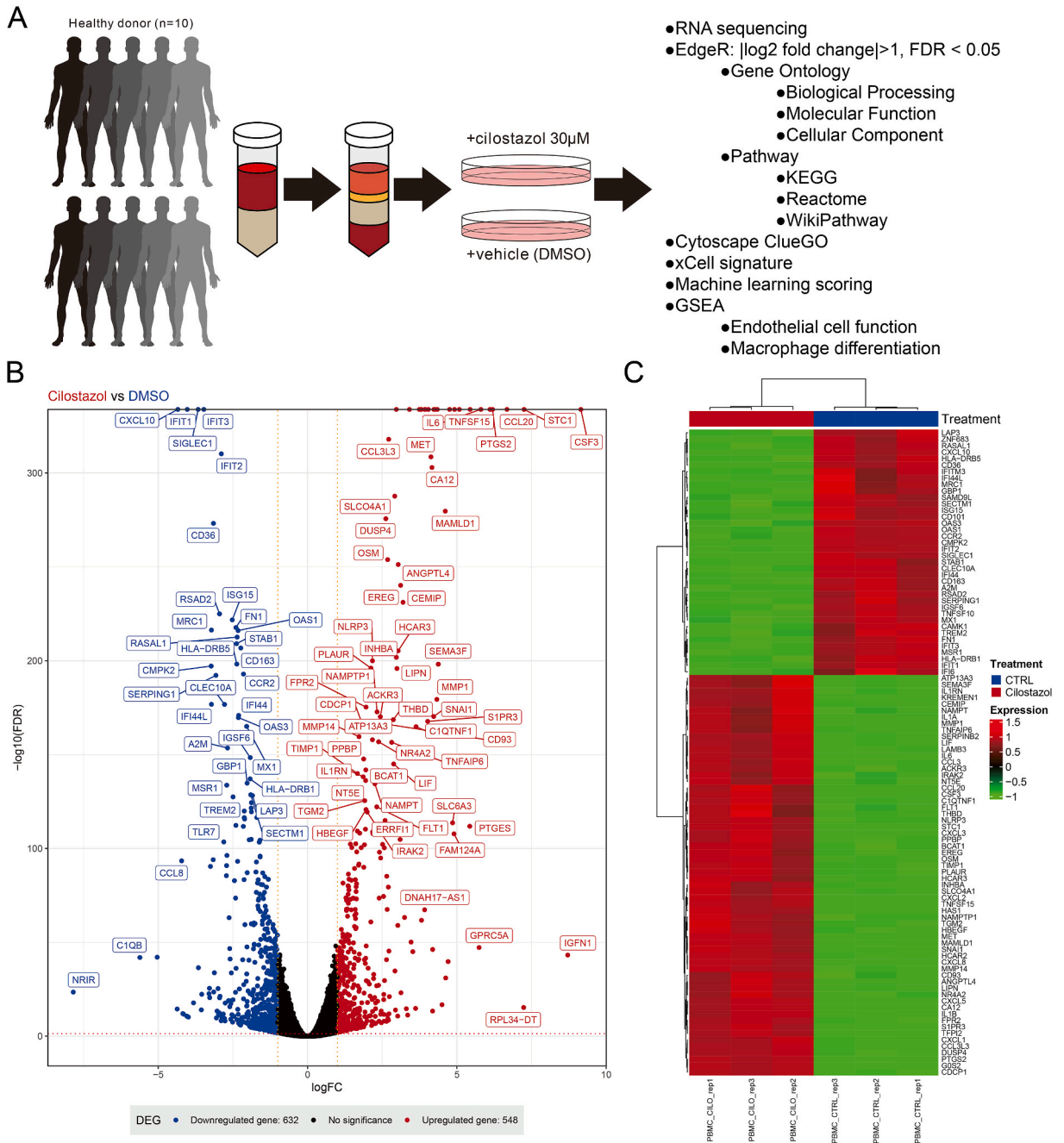


**Fig. 1. Analysis of cilostazol's effects on PBMCs.** A) Schematic diagram illustrating the study design. PBMCs from healthy donors were treated ex vivo with either vehicle (DMSO) or cilostazol, followed by RNA sequencing. Subsequent analyses involved differential gene expression analysis, Gene Ontology (GO) interpretation, pathway analysis, digital cytometry, machine learning approaches, and Gene Set Enrichment Analysis (GSEA). B) Volcano plot visualizing the differential gene expression between cilostazol and DMSO-treated PBMCs. The plot represents the  $-\log_{10}$  transformed adjusted p-values (y-axis) against the  $\log_2$  fold change (x-axis). Upregulated genes (548) are depicted in red and downregulated genes (632) in blue. C) Heatmap illustrating the expression levels of the top 100 genes with the smallest false discovery rate (FDR) upon cilostazol treatment. Each row corresponds to a gene, and each column represents a sample. The genes (rows) and samples (columns) were hierarchically clustered based on their expression profiles. The clustering process involved calculating the Euclidean distance between each pair of genes or samples and then grouping them using the average linkage method. This resulted in a dendrogram where closely related genes or samples are placed near each other. The color intensity in each cell reflects the expression level of the gene in that sample, with red indicating upregulation and green indicating downregulation. (For interpretation of the references to color in this figure legend, the reader is referred to the Web version of this article.)

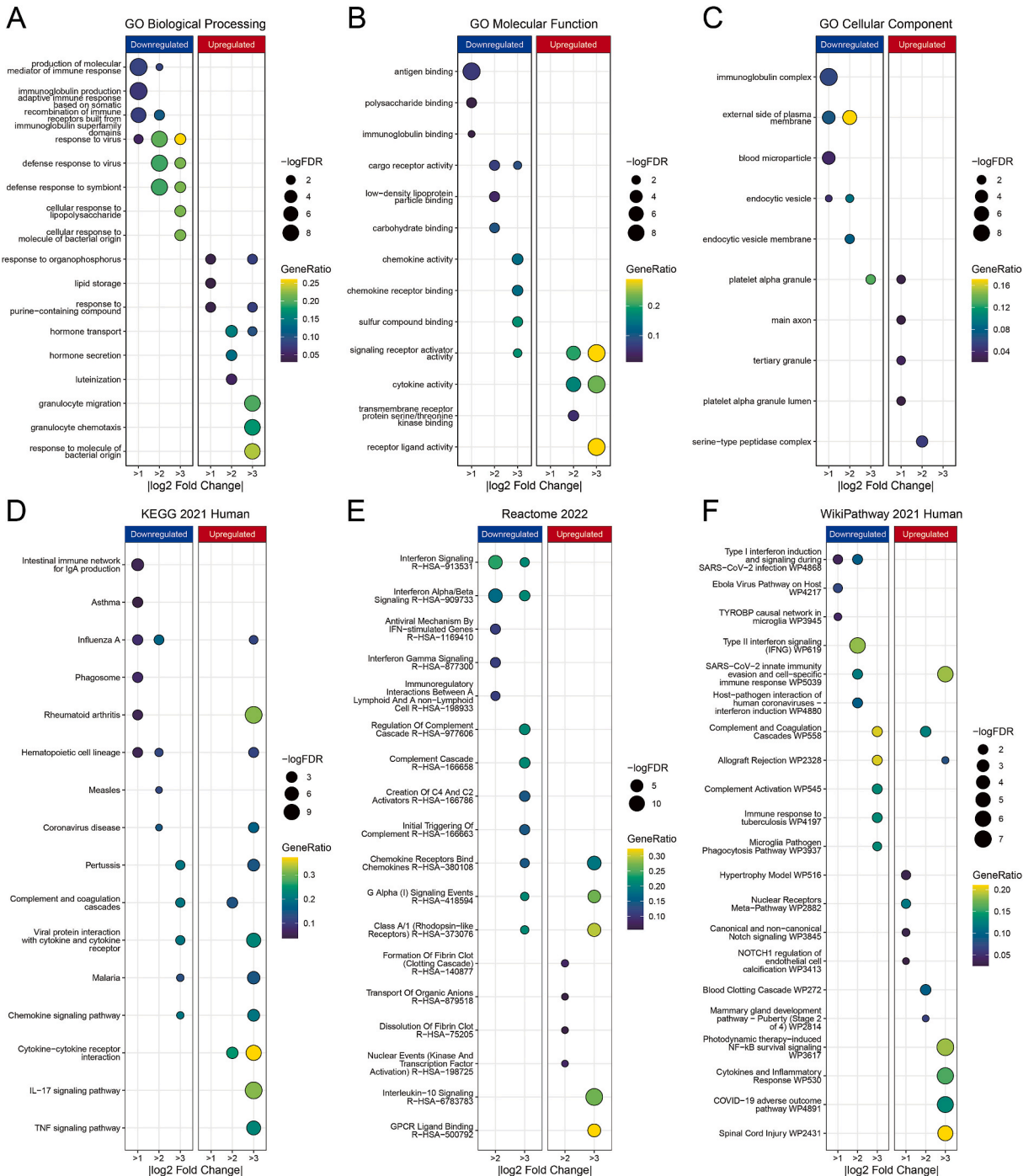


**Fig. 2. Over-Representation Analysis (ORA) of cilostazol's impact on gene expression.** Differentially expressed genes were screened based on  $|\log_2\text{FoldChange}| > 1,2,3$  and a false discovery rate (FDR)  $< 0.05$ . Downregulated genes are represented by blue bars, and upregulated genes by red bars. The analysis was performed using the compareCluster function of the clusterProfiler package. The size of the dots represents the  $-\log_{10}(\text{FDR})$ , indicating the significance of the gene set enrichment. The color of the dots, represented using the viridis color scale, indicates the proportion of differentially expressed genes (DEGs) in each gene set, with yellow indicating a higher proportion. The analysis covers (A) Gene Ontology Biological Process (GOBP), (B) Gene Ontology Molecular Function (GOMF), (C) Gene Ontology Cellular Component (GOCC), (D) Kyoto Encyclopedia of Genes and Genomes (KEGG), (E) Reactome, and (F) WikiPathway. (For interpretation of the references to color in this figure legend, the reader is referred to the Web version of this article.)

CD163-BV421 antibody (BioLegend, Inc., San Diego, CA, USA, Cat.: 333612), and CD206- PE/Dazzle™ 594 antibody (Biolegend, Cat.: 321130) were targeted to evaluate macrophage differentiation. After the incubation period, the cells were analyzed by flow cytometry using the Attune™ NxT Flow Cytometry (Thermo Fisher Scientific). to assess the fluorescence intensity of the markers. The variation in fluorescence intensity was utilized to quantify the expression levels of the specific differentiation markers, thereby evaluating the effect of cilostazol on the differentiation process.

## 4. Results

### 4.1. Exploring the impact of cilostazol on peripheral blood mononuclear cells

The present study investigated the effects of cilostazol on PBMCs using RNA sequencing (Fig. 1A). PBMCs from 10 healthy donors were treated ex vivo with vehicle control (DMSO) or cilostazol. The transcriptomic profile of the treated PBMCs was examined in detail by RNA sequencing. This high-dimensional transcriptomic data was subsequently analyzed using the edgeR package, specifically designed for differential expression analysis. This provided a list of genes that showed significant changes in expression upon cilostazol treatment. Gene Ontology (GO) analysis was used to interpret the differentially expressed genes, which covered three domains: biological processes, molecular functions, and cellular components, providing a comprehensive understanding of the biological context of the genes. Pathway analysis was performed using the Kyoto Encyclopedia of Genes and Genomes (KEGG), Reactome, and WikiPathway databases to gain insight into the complex network of biological pathways involving these genes. The Cytoscape ClueGO plugin, which provides interactive visual exploration of functionally grouped GO and pathway annotation networks, was used to present a clear picture of the relationships between enriched terms. In addition, xCell, a digital cytometry tool, was used to derive cell-type-specific signatures from the gene expression data, providing a comprehensive landscape of the cellular composition of the samples and helping to identify potential shifts in cell populations upon cilostazol treatment. Machine learning approaches were used to construct predictive models of treatment response based on gene expression profiles. Finally, GSEA focusing on endothelial cell function and macrophage differentiation was performed to determine whether predefined gene sets showed significant differences between the two biological states, thus improving our understanding of the effects of cilostazol on PBMCs.

Fig. 1B presents a volcano plot showcasing the differential gene expression between cilostazol and DMSO-treated PBMCs. Notably, 548 genes were found to be upregulated and 632 genes downregulated. Fig. 1C highlights the top 100 genes with the smallest false discovery rate (FDR). Several upregulated genes have been implicated in regulating immune responses and inflammation, such as *CSF3*, *CCL20*, *PTGS2*, *TNFSF15*, *IL6*, *HAS1*, *PTGES*, *IL1A*, and *IL1B*. These genes have been associated with different aspects of immune regulation, including cytokine production, chemotaxis, and inflammation, suggesting that cilostazol might modulate the immune environment. Among the downregulated genes, *MRC1*, *IFI44L*, *CMPK2*, *ANKRD22*, *HGF*, *CXCL11*, *IFIT3*, *SIGLEC1*, *C1QA*, *IFIT1*, *FST*, *IFI27*, *CCL8*, *CXCL10*, and *STEAP4*, stand out as they have been linked to various immune processes, including immune cell activation and recruitment and immune response to pathogens. Notably, genes like *MRC1*, *CXCL11*, *CXCL10*, and *C1QA* are well known for their roles in macrophage function, especially the M1 type, which is typically associated with inflammation and tissue damage. In particular, *MRC1* (CD206) is a well-established marker for M2 macrophages but is also expressed in a subset of M1 macrophages. The downregulation of *MRC1* may hint at a decrease in the population of these cells or a shift in the M1/M2 balance. Similarly, the chemokines *CXCL10* and *CXCL11* are involved in the recruitment of various immune cells, including M1 macrophages, to the sites of inflammation. Downregulation of these chemokines could result in decreased recruitment of these cells.

### 4.2. Evaluating the global impact of cilostazol through gene ontology and pathway analysis

In order to comprehensively analyze the potential impacts and biological responses of cilostazol regarding PBMCs, a differential gene expression analysis was conducted using edgeR. Genes upregulated and downregulated by cilostazol treatment were identified and categorized based on the absolute value of their log<sub>2</sub> fold change, with thresholds set at 1, 2, and 3. This allowed for a nuanced multi-cluster analysis of the gene expression changes. GO Biological Process analysis revealed that the downregulated genes were associated with several immune-related processes (Fig. 2A). These include the production of molecular mediators of immune response, immunoglobulin production, and adaptive immune response based on somatic recombination of immune receptors built from immunoglobulin superfamily domains. Other processes included defense response to viruses and symbionts and cellular responses to lipopolysaccharides and molecules of bacterial origin. Conversely, the upregulated genes were linked to response to organophosphorus, lipid storage, response to purine-containing compounds, hormone transport, hormone secretion, luteinization, granulocyte migration, granulocyte chemotaxis, and response to molecules of bacterial origin. GO Molecular Function analysis provided further insights into the potential function of cilostazol on PBMCs (Fig. 2B). The downregulated genes were associated with functions such as antigen binding, polysaccharide binding, immunoglobulin binding, cargo receptor activity, low-density lipoprotein particle binding, carbohydrate binding, chemokine activity, chemokine receptor binding, and sulfur compound binding. The upregulated genes were linked to functions such as signaling receptor activator activity, cytokine activity, transmembrane receptor protein serine/threonine kinase binding, and receptor-ligand activity. The GO Cellular Component analysis revealed that cilostazol primarily affects certain cellular structures (Fig. 2C). Downregulated genes are associated with the immunoglobulin complex, the external side of the plasma membrane, blood microparticles, endocytic vesicles, and platelet alpha granules. Upregulated genes are linked to the tertiary granule, platelet alpha granule lumen, and serine-type peptidase complex.

The KEGG analysis revealed that cilostazol significantly impacts various immune-related pathways (Fig. 2D). Downregulated pathways include those involved in the intestinal immune network for IgA production, phagosome function, hematopoietic cell

lineage, and the chemokine signaling pathway. Upregulated pathways include cytokine-cytokine receptor interaction and the IL-17 and TNF signaling pathways. Interestingly, the complement and coagulation cascades and viral protein interaction with cytokine and cytokine receptor pathways were both upregulated and downregulated, indicating the complex effect of cilostazol on these pathways. The Reactome pathway analysis provides further insights into the potential effects of cilostazol on cytokine signaling and function (Fig. 2E). The upregulated pathways are primarily associated with cytokine and chemokine signaling, including IL-10 signaling, chemokine receptors binding chemokines, signaling by interleukins, and IL-4 and IL-13 signaling. These pathways are crucial in immune response, inflammation, and cell communication. The downregulated pathways are mainly related to the interferon (IFN) signaling and complement cascade, including IFN signaling, IFN alpha/beta signaling, complement cascade regulation, complement cascade, C4 and C2 activator creation, initial triggering of complement, antiviral mechanism by IFN-stimulated genes, and IFN gamma signaling. These pathways are key components of the innate immune response, suggesting that cilostazol may modulate this aspect of immunity. The WikiPathways analysis provides further insights into the impact of cilostazol on various biological pathways (Fig. 2F). Notably, several pathways related to immune response and inflammation were found to be upregulated, including photodynamic therapy-induced NF-kB survival signaling, cytokines and inflammatory response, COVID-19 adverse outcome pathway, SARS-CoV-2 innate immunity evasion and cell-specific immune response, and IL-18 signaling pathways. These pathways play crucial roles in immune cell activation, communication, and response to pathogens, suggesting that cilostazol may enhance certain aspects of

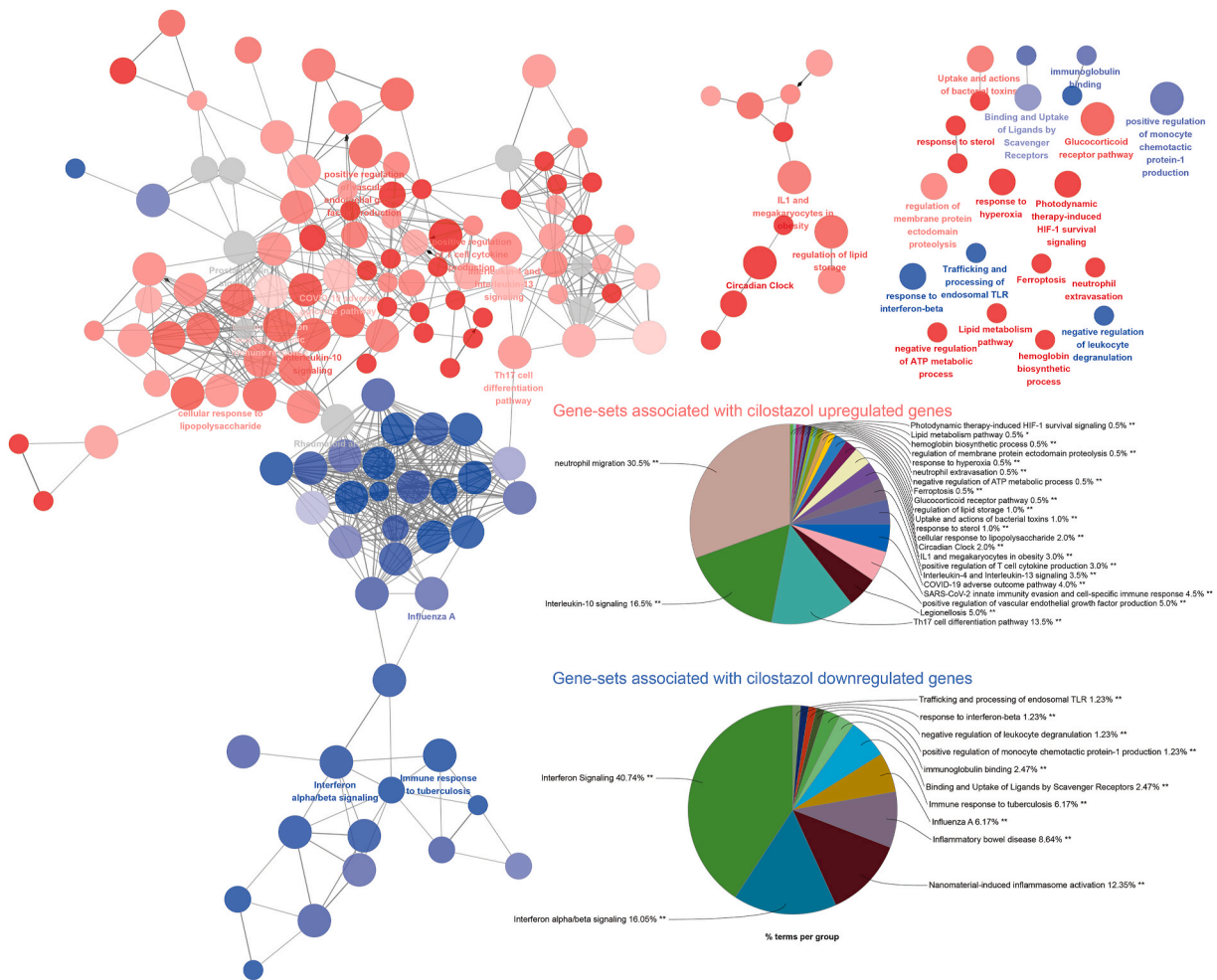


**Fig. 3. Network visualization of gene ontology and pathway analysis using Cytoscape ClueGO.** The network was generated using default settings, with upregulated gene sets represented by red clusters and downregulated gene sets represented by blue clusters. The size of each node corresponds to the ratio of genes in the gene set that are differentially expressed, with larger nodes indicating a higher ratio. The color intensity of each node reflects the false discovery rate (FDR) of the gene set, with darker colors indicating a smaller FDR. Edges between nodes represent shared genes between gene sets, with the length of the edges indicating the number of shared genes - shorter edges represent a higher number of shared genes. Pie charts represent the proportion of each gene set cluster in all upregulated or downregulated gene-associated gene sets. The percentage next to each term in the pie charts indicates the proportion of that term in the total gene set. Asterisks next to the terms represent the significance of the gene set, with one asterisk (\*) indicating a p-value <0.05, and two asterisks (\*\*) indicating a p-value <0.01. (For interpretation of the references to color in this figure legend, the reader is referred to the Web version of this article.)

immune response. However, the downregulated pathways are particularly interesting. The type II IFN signaling pathway, which plays a key role in antiviral defense and immune response modulation, was downregulated.

The comprehensive analysis of the effect of cilostazol on PBMCs suggests a significant modulation of immune responses.

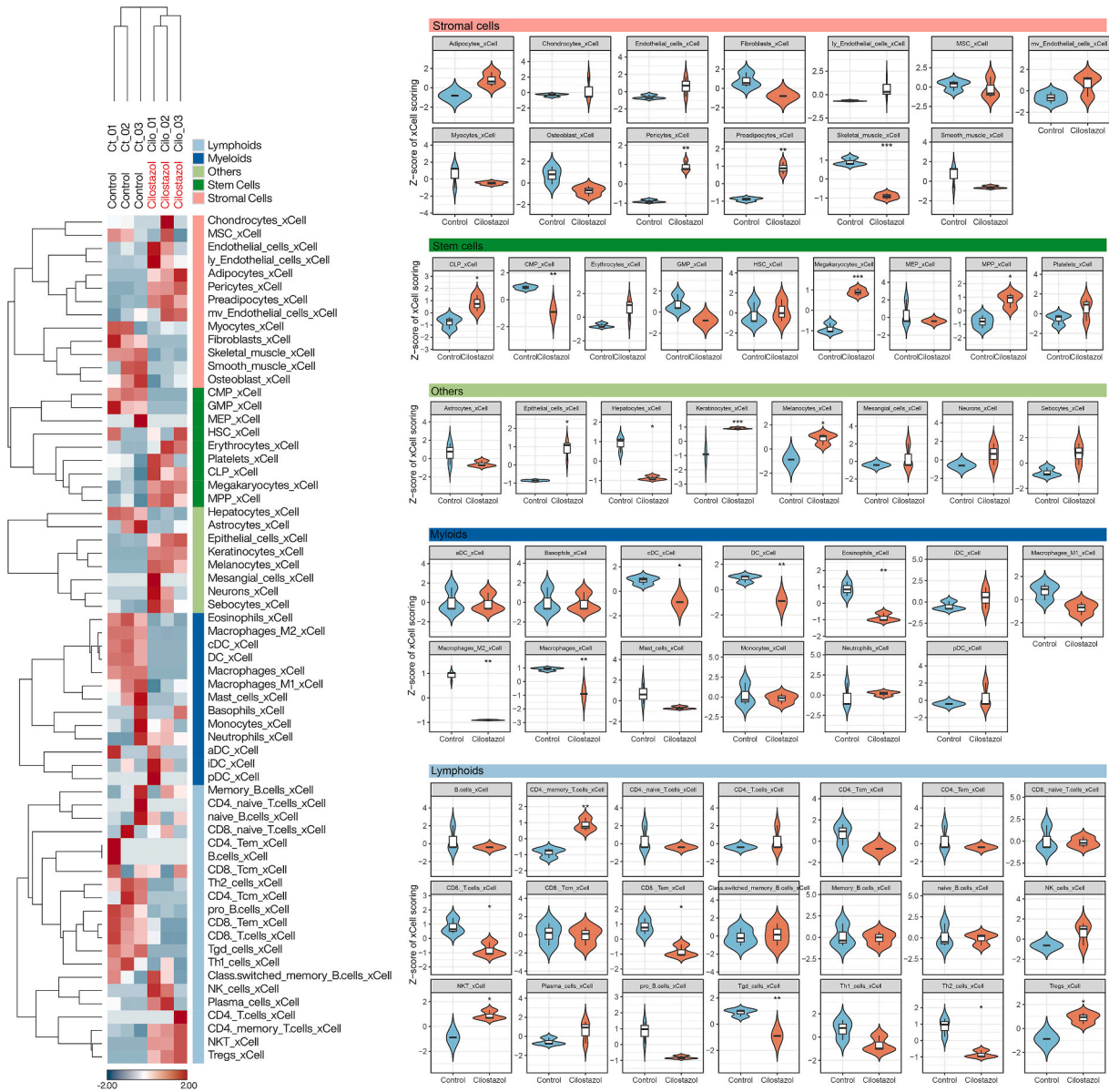


**Fig. 4.** xCell Analysis of PBMCs Treated with Cilostazol. The heatmap (left) displays the z-score of xCell scores for each identified cell type, with each row representing a cell type and each column representing a sample. The color intensity in each cell reflects the z-score of the xCell score for that cell type in the corresponding sample, with red indicating a higher score and blue indicating a lower score. The cell types are grouped into five categories: Stromal (pink), Stem Cells (dark green), Others (light green), Myeloids (blue), and Lymphoids (light blue), and are clustered hierarchically based on Euclidean distance. The violin plots (right) show the distribution of z-scores for each cell type within the five categories. Inside each violin plot, a boxplot is embedded. The box represents the interquartile range (IQR), the line inside the box marks the median, and the whiskers extend to the smallest and largest values. Statistical significance between the cilostazol-treated and untreated groups was determined using a *t*-test, with \* indicating a p-value < 0.05, \*\* indicating a p-value < 0.01, and \*\*\* indicating a p-value < 0.001. The abbreviations used for the cell types are as follows: ly\_endothelial cell (Lymphatic Endothelial Cell), iDC (Immature Dendritic Cell), pDC (Plasmacytoid Dendritic Cell), aDC (Activated Dendritic Cell), MSC (Mesenchymal Stem Cell), mv\_endothelial cell (Microvascular Endothelial Cell), CLP (Common Lymphoid Progenitor), CMP (Common Myeloid Progenitor), GMP (Granulocyte-Macrophage Progenitor), HSC (Hematopoietic Stem Cell), MEP (Megakaryocyte-Erythroid Progenitor), MPP (Multipotent Progenitor), Tem (Effector Memory T Cell), Tgd (Gamma Delta T Cell), NK (Natural Killer Cell), NKT (Natural Killer T Cell), Tcm (Central Memory T Cell), Treg (Regulatory T Cell). (For interpretation of the references to color in this figure legend, the reader is referred to the Web version of this article.)

Downregulated genes and pathways are predominantly associated with key aspects of adaptive and innate immunity, including antigen binding, immunoglobulin production, and IFN signaling. This suggests that cilostazol may exert an immunosuppressive effect, potentially reducing the body’s ability to respond to pathogens. However, the upregulation of certain immune-related pathways, particularly those involved in cytokine signaling, suggests a complex, multifaceted impact on immune function.

4.3. Integrated analysis suggests immunosuppressive effects of cilostazol on PBMCs

A visual distribution map was created using Cytoscape ClueGO to comprehensively evaluate the significant results of GO and Pathway analyses (Fig. 3). This map was color-coded, with red and blue marking the upregulated and downregulated differentially expressed gene-associated gene sets, respectively. The map revealed a considerable overlap among many associated gene sets, indicating shared genes and pathways. Pie charts were created to further assess the proportion of upregulated and downregulated differentially expressed genes associated with gene sets. The top three upregulated gene set clusters were neutrophil migration (30.5%), IL-10 signaling (16.5%), and the Th17 cell differentiation pathway (13.5%). However, the top three downregulated gene set clusters were IFN signaling (40.74%), IFN alpha/beta signaling (16.05%), and nanomaterial-induced inflammasome activation (12.35%). These findings suggest that while inflammation-related IFN pathways were present in both upregulated and downregulated

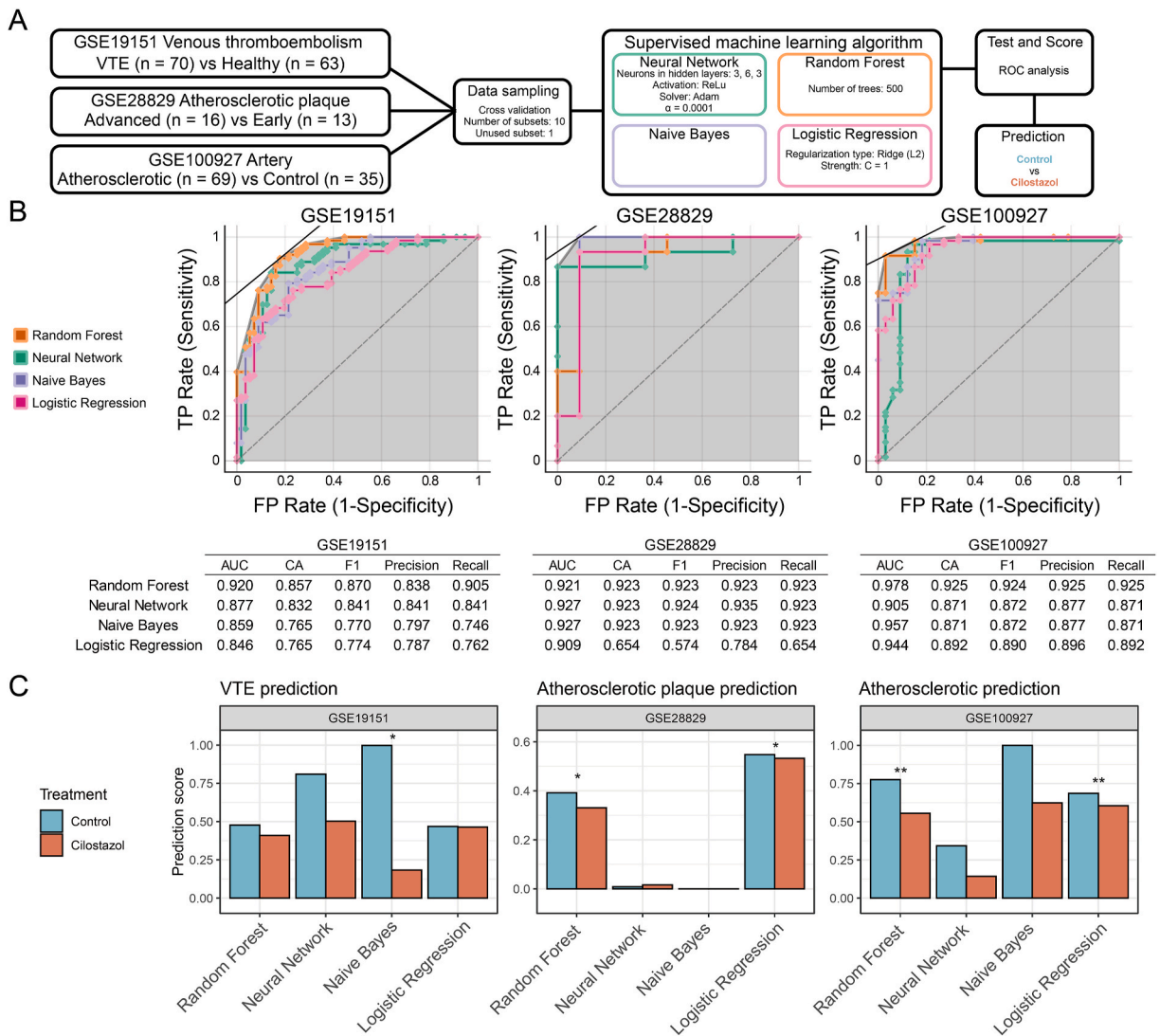


**Fig. 5. Machine Learning Analysis of Cilostazol’s Impact on Cardiovascular Disease Prediction.** A) Flowchart illustrating the process of machine learning training and prediction. B) Receiver Operating Characteristic (ROC) analysis and Score. True Positive Rate (TP Rate), False Positive Rate (FP Rate), Area Under the Curve (AUC), Classification Accuracy (CA), F1 Score, Precision, and Recall are presented. C) Barplot representing the predicted disease scores for each database. The data are presented as the mean values of three sample groups after prediction. The significance of differences between groups was calculated using the *t*-test, with \* indicating  $p < 0.05$  and \*\* indicating  $p < 0.01$ .

tendencies, cilostazol primarily appears to exert an anti-inflammatory effect by downregulating these pathways. This is particularly relevant in CVDs, as chronic inflammation is a key driver of atherosclerosis, a condition characterized by the buildup of plaques in the arteries. Interestingly, the upregulation of IL-10 signaling and Th17 cell differentiation pathways, which accounted for significant proportions of the upregulated gene sets, may have implications for atherosclerosis. IL-10 is a potent anti-inflammatory cytokine that can inhibit the synthesis of proinflammatory cytokines and prevent atherogenesis [38,39]. Similarly, Th17 cells, a subset of T-helper cells, have been implicated in regulating inflammation and autoimmunity. Although their protective role in atherosclerosis is still being researched [40], it has been suggested that Th17 cells may reduce immune cell adhesion by modulating the expression of VCAM1, a key molecule involved in the adhesion of leukocytes to the vascular endothelium. This modulation could potentially be linked to the observed changes in neutrophil migration.

4.4. xCell analysis reveals the role of cilostazol role in inhibiting monocyte differentiation and promoting endothelial cell function

To assess the impact of cilostazol on PBMC composition, we utilized xCell, a computational tool that can simulate and analyze the cellular composition of 64 different cell types. Following the original authors' suggestions, all results were divided into five categories: lymphoids, myeloids, stem cells, stromal cells, and others. A heatmap was generated to visualize the distribution of score differences caused by cilostazol treatment, with individual cell group comparisons presented in violin plots on the right (Fig. 4). Notably, the stromal cell category showed an increase in specific cell populations following cilostazol treatment. These included endothelial cells, ly\_endothelial cells, adipocytes, pericytes, preadipocytes, and mv\_endothelial cells. In contrast, the myeloid category showed a general

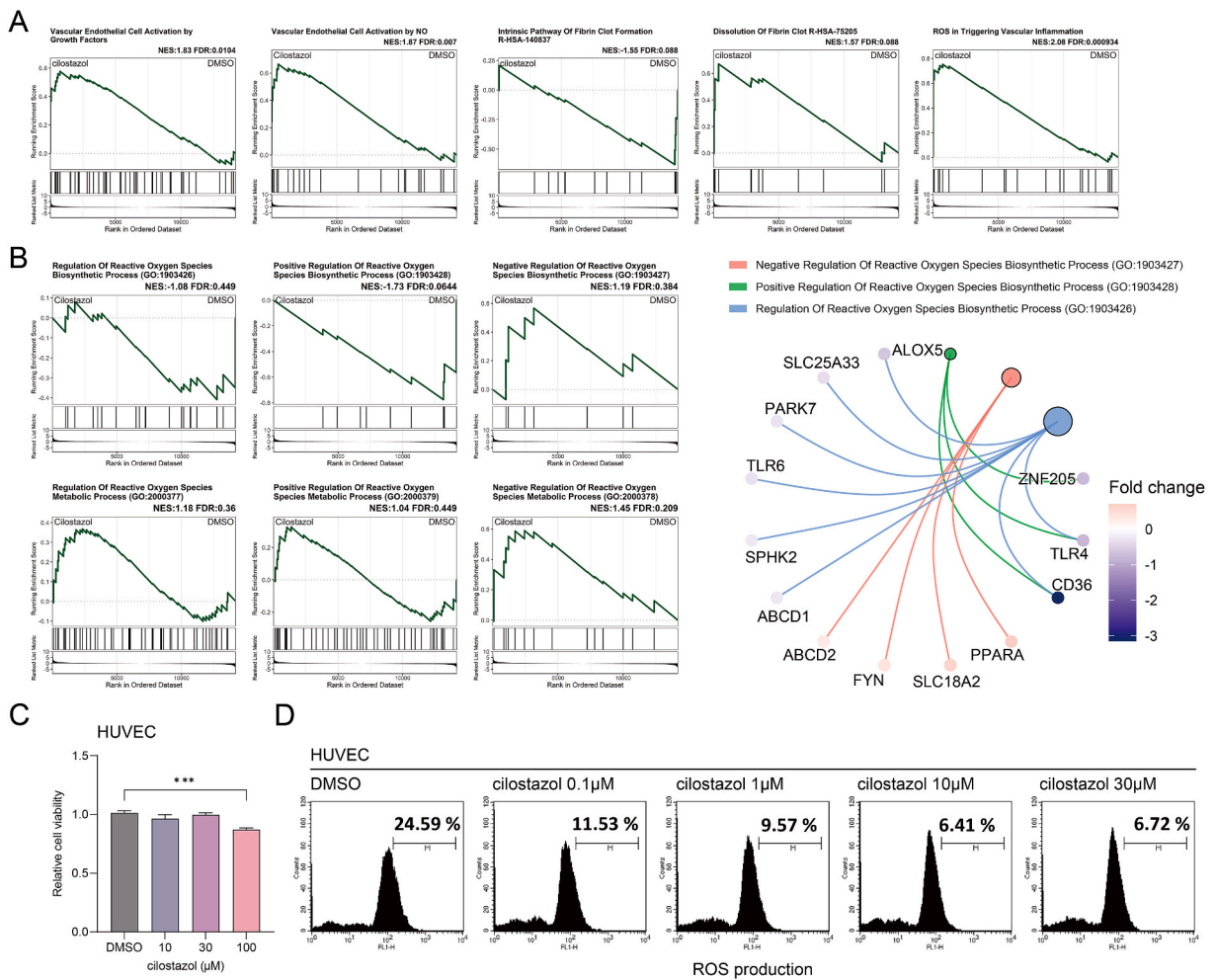


**Fig. 6. GSEA plot and Experimental Validation of Cilostazol's Impact on ROS Production and Endothelial Cell Viability.** A) GSEA reveals the enrichment of several gene sets related to endothelial cell activation and fibrin clot formation. B) GSEA plot and CNET plot indicate the enrichment of gene sets related to the biosynthetic process of Reactive Oxygen Species (ROS), highlighting the leading edge genes. C) The results of a cell viability assay for HUVEC treated with different concentrations of cilostazol are presented. The results indicate that \*\*\* has a significantly lower P value (*t*-test,  $P < 0.001$ ) compared to DMSO. D) Flow cytometry was used to analyze ROS production in HUVEC following 24-h treatment with cilostazol.



**Fig. 7. GSEA Plot and Experimental Validation of Cilostazol's Impact on Macrophage Behavior and Trends of Differentiation.** A) Summarized circular GSEA NES plot revealing the enrichment of selected gene sets related to macrophage biological behaviors. Red bar indicates positive enrichment, blue bar indicates negative enrichment, black text represents FDR <0.25 (indicating significance), and gray text denotes an FDR that is not significant. Statistical significance is further denoted by \*: FDR <0.05, \*\*: FDR <0.01. B) GSEA plot representing the association with macrophage subtypes in peripheral blood, sourced from the CellMarker database. C) CNET plot showcasing the enrichment of gene sets pertinent to macrophage subtypes in peripheral blood, with an emphasis on the leading edge genes; the corresponding heatmap arranges leading edge genes in alphabetical order. D) Flow cytometry analysis of macrophage biomarkers in the THP-1 cell line following a 24-h treatment with cilostazol, compared to DMSO; statistical significance denoted by \*\*\*\*:  $p < 0.0001$ . (For interpretation of the references to color in this figure legend, the reader is referred to the Web version of this article.)

atherosclerosis management [41]. These findings provide valuable insights into the immunomodulatory effects of cilostazol on PBMCs. The observed changes in cell composition suggest that cilostazol may exert its effects by modulating the balance of various immune cell populations. The increase in stromal cells, particularly endothelial cells and adipocytes, could enhance vascular health and lipid metabolism, respectively. The decrease in myeloid cells, particularly dendritic cells and macrophages, could reduce inflammation and immune response, potentially mitigating the immune-mediated damage associated with CVDs. These changes align with the previously observed downregulation of inflammation-related pathways and upregulation of anti-inflammatory and protective pathways, further supporting the potential therapeutic benefits of cilostazol in CVDs.

#### 4.5. Exploring the potential of cilostazol in alleviating cardiovascular diseases through supervised Machine Learning Analysis

To understand the substantive effects of cilostazol on healthy donor PBMCs and their association with clinical CVD, we used the xCell approach to analyze three datasets providing patient data for cardiovascular conditions. These datasets were GSE19151, GSE28829, and GSE100927, each representing a different CVD target group: venous thromboembolism (VTE) vs. healthy donors, advanced vs. early atherosclerotic plaque, and atherosclerotic vs. control artery, respectively. We classified the original data into binary categories and used 10-fold cross-validation to train our models for sample selection. Our approach involved four supervised machine learning algorithms: random Forest, Neural Network, Naïve Bayes, and Logistic Regression. These were used to predict the relative scores of PBMCs identified as diseased following cilostazol treatment (Fig. 5A). Fig. 5B shows the predictive ability of the four algorithms for each disease group in the databases, demonstrating that the area under the curve for all reached nearly 0.9, indicating high accuracy. After training, the algorithms were used to estimate scores for samples with and without cilostazol treatment. The results showed that after cilostazol treatment, the scores for being classified as VTE, advanced atherosclerotic plaque, or atherosclerotic artery all decreased to varying degrees (Fig. 5C). This suggests that cilostazol can alleviate CVD progression.

#### 4.6. Analysis of gene set enrichment provides insight into the role of cilostazol in regulating reactive oxygen species and endothelial cell activation

A previous study showed that cilostazol activates eNOS and TM expression through the KLF2 pathway, indicating its potential antithrombotic and vascular protective effects on endothelial cells (Reference: 34638626). Our analysis included the GSEA strategy to identify relevant gene sets. The findings revealed positive enrichment for gene sets related to "Vascular Endothelial Cell Activation by Growth Factor" (normalized enrichment score [NES]: 1.83, FDR: 0.0104), "Vascular Endothelial Cell Activation by NO" (NES: 1.87, FDR: 0.007), and "Dissolution of Fibrin Clot R-HSA-75205" (NES: 1.57, FDR: 0.088). In contrast, the gene set related to "Intrinsic Pathway of Fibrin Clot Formation R-HAS-140837" (NES: 1.55, FDR: 0.088) had negative enrichment, consistent with the experimental results in HUVEC (Fig. 6A). A significant correlation was found between cilostazol treatment and the "ROS in Triggering Vascular Inflammation" gene set (NES: 2.08, FDR: 0.000934). To comprehend the association between cilostazol and the production/metabolism of reactive oxygen species (ROS), we searched for gene sets from GO for GSEA, which are related to the regulation of ROS production and metabolism. Amongst all, only "Positive Regulation of Reactive Oxygen Species Biosynthetic Process (GO:1903428)" displayed negative enrichment (NES: 1.73, FDR: 0.0644). The GO term, "Negative Regulation of Reactive Oxygen Species Biosynthetic Process (GO:1903427)," did not reach statistical significance but showed positive enrichment (NES: 1.19, FDR: 0.384). This suggests that cilostazol treatment can inhibit ROS biosynthesis in endothelial cells (see Fig. 6B, Left panel). The genes at the leading edge of the "ROS Biosynthetic Process" were plotted using the cnetplot function of clusterProfiler (Fig. 6B Right panel). The leading-edge genes in this group are *ZNF205*, *TLR4*, and *CD36*, known for their roles in causing oxidative stress and inflammation. *TLR4* activates an immune response, while *CD36* promotes foam cell formation within atherosclerotic plaques. In contrast, the gene set that negatively regulates reactive oxygen species biosynthesis shows a positive NES, indicating an increase in genes that suppress ROS production. The set comprises *PPARA*, *SLC18A2*, *FYN*, and *ABCD2* as core genes. *PPARA* deserves special attention as it affects lipid metabolism and inflammation, which are crucial in the development of atherosclerosis. Finally, the gene set "Regulation of Reactive Oxygen Species Biosynthetic Process" displayed a negative NES, suggesting a general reduction in the regulation of ROS production. The set consists of core genes *ABCD1*, *SPHK2*, *TLR6*, *PARK7*, *SLC25A33*, *ALOX5*, *TLR4*, and *CD36*. These genes participate in various processes such as inflammation, lipid metabolism, and oxidative stress response, collectively contributing significantly to the development of atherosclerosis. We additionally exposed HUVEC to DMSO, 10  $\mu$ M, 30  $\mu$ M, and 100  $\mu$ M cilostazol, revealing that up to 30  $\mu$ M does not hinder the growth activity of HUVEC (Fig. 6C). By employing H2CFDA to evaluate ROS production, we observed that an increase in cilostazol effectively suppressed ROS production (Fig. 6D), corroborating our findings in transcriptomics.

#### 4.7. Inhibitory effects of cilostazol on macrophage differentiation evidenced by Gene Set Enrichment Analysis

To understand the effect of cilostazol on macrophage differentiation, we used the MGI mammalian database to filter for “macrophage,” resulting in 16 gene sets describing the biological behavior of macrophages. Fig. 7A shows the NES and significance of the 16 gene sets after GSEA. Among them, “abnormal macrophage chemotaxis MP:0010760” (NES:  $-1.87$ , FDR: 0.0145), “abnormal alveolar macrophage morphology MP:0008245” (NES: 1.66, FDR: 0.0257), “decreased macrophage cell number MP:0003884” (NES: 1.51, FDR: 0.121), and “impaired macrophage phagocytosis MP:0001798” (NES: 1.4, FDR: 0.228) were significantly negatively enriched, suggesting that cilostazol affects macrophage function. We also used the Cell Marker database to filter for “peripheral blood” and “macrophage,” resulting in three gene sets. GSEA showed that cilostazol treatment was significantly negatively enriched for “Macrophage: Peripheral Blood” (NES: 1.64, FDR: 0.00587), “M1 macrophage: Peripheral Blood” (NES: 1.83, FDR: 0.00461), and “M2 macrophage: Peripheral Blood” (NES: 1.16, FDR: 0.103), suggesting that cilostazol may inhibit the differentiation of monocytes into macrophages (Fig. 7B). The leading-edge genes of the three gene sets were presented using the cnet and heat plots, showing that all genes related to macrophages were downregulated under cilostazol treatment (Fig. 7C). To validate the effect of cilostazol on macrophage-related biomarkers, we treated THP-1 cells with 30  $\mu\text{M}$  cilostazol for 48 h and evaluated the expression of M1 marker CD80 and M2 markers CD163 and CD206. The results showed that cilostazol effectively reduced the biomarkers of both M1 and M2 macrophages, confirming that cilostazol can inhibit the differentiation of monocytes into macrophages.

### 5. Discussion

The comprehensive analysis of the effect of cilostazol on PBMCs and its potential role in mitigating CVD presents several intriguing areas of discussion. The study discovered that the influence of cilostazol on PBMCs highlights its potential role in enhancing vascular health and regulating lipid metabolism. A notable increase in stromal cells, including endothelial cells and adipocytes, implies a synergistic approach to cardiovascular health [42]. Our previous study consistently supported the activation of KLF2 expression and its associated endothelial functions (eNOS activation, NO production, and TM secretion) by cilostazol [24]. Such evidence emphasizes its ability to inhibit oxidative stress-induced premature senescence and Sirt1 upregulation in human endothelial cells [43]. The findings from different studies further extend the understanding of the impact of cilostazol on lipid metabolism. It potentiates adipocyte differentiation in 3T3-L1 cells [44], and its effect on plasma lipoproteins in patients with intermittent claudication has also been noted [45]. Conversely, the influence of cilostazol on specific immune cells like dendritic cells and macrophages indicates reduced inflammation, a critical factor in CVD [46–49]. Its anti-inflammatory attributes are further affirmed in various scenarios, including hindlimb ischemia in a mouse model [50], potential COVID-19 treatment [51], and the inactivation of NF- $\kappa$ B in BV2 microglial cells [52]. This aligned evidence consolidates cilostazol's potential therapeutic value.

The analysis of gene expression changes induced by cilostazol in PBMCs highlights its complex immunomodulatory role, which is crucial for understanding its effects on CVDs. The gene downregulation related to antigen and immunoglobulin binding, alongside IFN signaling, positions cilostazol as a potential immunosuppressant. This observation is particularly relevant in the context of CVD, where elevated total serum IgE levels are associated with increased cardiovascular mortality risk in older adults [53], and serum antigen-specific IgE shows a significant association with CVD independent of traditional risk factors [54]. The impact on IFN signaling pathways is also noteworthy, considering the critical role of IFNs in atherosclerosis and related cardiovascular conditions [55–57]. Furthermore, the modulation of Th17 and Treg cells by cilostazol mirrors evidence suggesting an imbalance in these cell types is linked to CVDs, highlighting its potential in addressing pro-inflammatory states and vascular damage [58–60].

The anti-inflammatory potential of cilostazol, marked by the upregulation of IL-10 signaling, aligns with its proposed therapeutic role in cardiovascular disorders characterized by inflammation. The regulatory effect of IL-10 on inflammation and its correlation with CVD progression is complemented by the dual role of IL-17 in atherosclerosis [61–66]. The influence of cilostazol on macrophage polarization is also of significant interest; macrophage phenotype shifts in epicardial adipose tissue are closely associated with atherosclerosis [67,68]. Additionally, the influence of CXCL10 by cilostazol suggests its potential in conditions like ischemic stroke, where elevated levels of these chemokines are observed [69]. The modulation of Fc gamma receptors and their involvement in atherogenesis indicates a further therapeutic angle for cilostazol in CVD management [70–72]. Moreover, the impact of cilostazol on CD163 highlights its role in the broader spectrum of cardiovascular health [73].

A critical aspect of the study explored the role of cilostazol in controlling ROS and endothelial cell activation. The findings suggested a balanced mechanism, inhibiting ROS biosynthesis and promoting protective genes, offering potential antithrombotic and vascular protective effects [74,75]. Also, the inhibitory effects of cilostazol on macrophage differentiation contribute to understanding its immunomodulatory roles. The integration of supervised machine learning provided a novel perspective, accurately predicting the relative scores of PBMCs identified as diseased following cilostazol treatment. This high level of accuracy underlines the potential of cilostazol as a therapeutic agent, warranting further clinical exploration. While these findings present a comprehensive analysis of the therapeutic potential of cilostazol, some limitations must be acknowledged. The reliance on computational tools and *in vitro* models may not accurately mimic complex biological interactions within human organisms. Techniques like the xCell approach and GSEA, although valuable, may be susceptible to biases or inaccuracies. Furthermore, the machine learning applications need further validation with more diverse patient data to ensure robustness.

### 6. Conclusion

The comprehensive role of cilostazol in cardiovascular health, highlighted through extensive research, emphasizes the need for

further clinical investigation. Its influence on PBMCs, endothelial function, lipid metabolism, and anti-inflammatory pathways demonstrates its potential as a versatile therapeutic agent in CVD management. Its capability to regulate ROS particularly underscores its protective role against vascular dysfunction. Additionally, the application of advanced machine learning techniques to predict the therapeutic effects of cilostazol showcases its promise in personalized medicine for cardiovascular care. The insights into the immunomodulatory effects of cilostazol, especially its potential as an immunosuppressant, align with the increasing recognition of immune response dysregulation in cardiovascular pathologies. Therefore, cilostazol, with its myriad of benefits, warrants further exploration in both in vitro and in vivo studies to substantiate these findings and enhance patient outcomes in cardiovascular therapy.

### **Ethics approval and consent to participate**

Ethics approval for this study was obtained from the institutional review boards of both the Tri-Service General Hospital and the Taipei Veteran General Hospital, under IRB number 2012-03-001AC. The study protocols were designed in accordance with the ethical guidelines of the 1975 Helsinki Declaration. All participants were provided with comprehensive information about the study and voluntarily provided their written informed consent to participate.

### **Consent for publication**

Consent to publish has been obtained from all authors.

### **Funding**

This study was supported by TYAFGH-D110052 and TYAFGH\_E\_112052 from Taoyuan Armed Forces General Hospital (to CN Fan), the Ministry of National Defense-Medical Affairs Bureau (MND-MAB-112-112 to YL Chiu), Tri-Service General Hospital (TSGH-E-112205 to TN Tsai), and National Science and Technology Council, Taiwan (R.O.C.) under Grant no. NSTC 111-2314-B-016-019-MY3 (to YL Chiu).

### **Data availability statement**

The data supporting the findings of this study are available in the NCBI Gene Expression Omnibus (GEO) database under the accession number GSE250020.

### **CRedit authorship contribution statement**

**Chia-Ning Fan:** Writing – review & editing, Writing – original draft. **Tsung-Neng Tsai:** Supervision, Resources, Funding acquisition, Data curation. **Xin-Jie Lu:** Formal analysis, Data curation. **Hsing-Fan Lai:** Formal analysis, Data curation. **Chun-Hua Wang:** Formal analysis, Data curation. **Yi-Lin Chiu:** Writing – review & editing, Writing – original draft, Visualization, Validation, Supervision, Funding acquisition, Data curation, Conceptualization.

### **Declaration of competing interest**

The authors declare the following financial interests/personal relationships which may be considered as potential competing interests: Chia-Ning Fan reports financial support was provided by Taoyuan Armed Forces General Hospital (TYAFGH-D110052 and TYAFGH\_E\_112052). Tsung-Neng Tsai reports financial support was provided by Tri-Service General Hospital, National Defense Medical Center (TSGH-E-112205). Yi-Lin Chiu reports financial support was provided by National Science and Technology Council, Taiwan (R.O.C.) (NSTC 111-2314-B-016-019-MY3) and the Ministry of National Defense-Medical Affairs Bureau (MND-MAB-112-112). If there are other authors, they declare that they have no known competing financial interests or personal relationships that could have appeared to influence the work reported in this paper.

### **Acknowledgement**

Cilostazol was kindly provided by Yung Shin Pharmaceutical Industrial Co., Ltd. (Taiwan).

### **Appendix A. Supplementary data**

Supplementary data to this article can be found online at <https://doi.org/10.1016/j.heliyon.2024.e29194>.

## References

- [1] M. Vaduganathan, et al., The global burden of cardiovascular diseases and risk: a compass for future health, *J. Am. Coll. Cardiol.* 80 (25) (2022) 2361–2371.
- [2] J. Frostegard, Immunity, atherosclerosis and cardiovascular disease, *BMC Med.* 11 (2013) 117.
- [3] V.M. Victor, et al., Oxidative stress, endothelial dysfunction and atherosclerosis, *Curr Pharm Des* 15 (26) (2009) 2988–3002.
- [4] J. Frostegard, et al., Cytokine expression in advanced human atherosclerotic plaques: dominance of pro-inflammatory (Th1) and macrophage-stimulating cytokines, *Atherosclerosis* 145 (1) (1999) 33–43.
- [5] G. Camejo, et al., Characterization and properties of a lipoprotein-complexing proteoglycan from human aorta, *Atherosclerosis* 35 (3) (1980) 307–320.
- [6] J. Frostegard, et al., Oxidized low density lipoprotein induces differentiation and adhesion of human monocytes and the monocytic cell line U937, *Proc Natl Acad Sci U S A* 87 (3) (1990) 904–908.
- [7] J.A. Berliner, et al., Minimally modified low density lipoprotein stimulates monocyte endothelial interactions, *J. Clin. Invest.* 85 (4) (1990) 1260–1266.
- [8] K.J. Moore, F.J. Sheedy, E.A. Fisher, Macrophages in atherosclerosis: a dynamic balance, *Nat. Rev. Immunol.* 13 (10) (2013) 709–721.
- [9] B.A. Ference, et al., Low-density lipoproteins cause atherosclerotic cardiovascular disease. 1. Evidence from genetic, epidemiologic, and clinical studies. A consensus statement from the European Atherosclerosis Society Consensus Panel, *Eur. Heart J.* 38 (32) (2017) 2459–2472.
- [10] R. Ross, J.A. Glomset, The pathogenesis of atherosclerosis (first of two parts), *N. Engl. J. Med.* 295 (7) (1976) 369–377.
- [11] H.J. Hsieh, et al., Shear-induced endothelial mechanotransduction: the interplay between reactive oxygen species (ROS) and nitric oxide (NO) and the pathophysiological implications, *J. Biomed. Sci.* 21 (1) (2014) 3.
- [12] R.M. Restaino, et al., Increased monocyte-derived reactive oxygen species in type 2 diabetes: role of endoplasmic reticulum stress, *Exp. Physiol.* 102 (2) (2017) 139–153.
- [13] Y. Zhang, et al., ROS play a critical role in the differentiation of alternatively activated macrophages and the occurrence of tumor-associated macrophages, *Cell Res.* 23 (7) (2013) 898–914.
- [14] K. Schror, The pharmacology of cilostazol, *Diabetes Obes Metab* 4 (Suppl 2) (2002) S14–S19.
- [15] Y.J. Lee, N.K. Je, Long-term effectiveness and safety of cilostazol versus clopidogrel in secondary prevention of noncardioembolic ischemic stroke, *Eur. J. Clin. Pharmacol.* 79 (8) (2023) 1107–1116.
- [16] Y. Ahn, et al., Randomized comparison of cilostazol vs clopidogrel after drug-eluting stenting in diabetic patients—cilostazol for diabetic patients in drug-eluting stent (CIDES) trial, *Circ. J.* 72 (1) (2008) 35–39.
- [17] C.M. Pratt, Analysis of the cilostazol safety database, *Am. J. Cardiol.* 87 (12A) (2001) 28D–33D.
- [18] J.L. Lin, et al., A randomized controlled trial evaluating outcome impact of cilostazol in patients with coronary artery disease or at a high risk of cardiovascular disease, *J Pers Med* 12 (6) (2022).
- [19] H. Ueno, et al., Comparison of the effect of cilostazol with aspirin on circulating endothelial progenitor cells and small-dense LDL cholesterol in diabetic patients with cerebral ischemia: a randomized controlled pilot trial, *J Atheroscler Thromb* 18 (10) (2011) 883–890.
- [20] J.H. Lee, et al., Addition of cilostazol reduces biological aspirin resistance in aspirin users with ischaemic stroke: a double-blind randomized clinical trial, *Eur. J. Neurol.* 17 (3) (2010) 434–442.
- [21] S. Uchiyama, et al., Stroke prevention by cilostazol in patients with atherothrombosis: meta-analysis of placebo-controlled randomized trials, *J. Stroke Cerebrovasc. Dis.* 18 (6) (2009) 482–490.
- [22] T.H. Lee, et al., Comparison of long-term efficacy and safety between cilostazol and clopidogrel in chronic ischemic stroke: a nationwide cohort study, *Ther Adv Chronic Dis* 11 (2020) 2040622320936418.
- [23] Y.L. Chiu, et al., Ginkgo biloba induces thrombomodulin expression and tissue-type plasminogen activator secretion via the activation of kruppel-like factor 2 within endothelial cells, *Am. J. Chin. Med.* 48 (2) (2020) 357–372.
- [24] C.H. Wu, et al., Cilostazol induces eNOS and TM expression via activation with sirtuin 1/Kruppel-like factor 2 pathway in endothelial cells, *Int. J. Mol. Sci.* 22 (19) (2021).
- [25] T.N. Tsai, et al., Activation of kruppel-like factor 2 with ginkgo biloba extract induces eNOS expression and increases NO production in cultured human umbilical endothelial cells, *Acta Cardiol. Sin.* 30 (3) (2014) 215–222.
- [26] A. Frankish, et al., GENCODE reference annotation for the human and mouse genomes, *Nucleic Acids Res.* 47 (D1) (2019) D766–D773.
- [27] F.J. Martin, et al., Ensembl 2023, *Nucleic Acids Res.* 51 (D1) (2023) D933–D941.
- [28] T. Wu, et al., clusterProfiler 4.0: a universal enrichment tool for interpreting omics data, *Innovation* 2 (3) (2021) 100141.
- [29] E.Y. Chen, et al., Enrichr: interactive and collaborative HTML5 gene list enrichment analysis tool, *BMC Bioinf.* 14 (2013) 128.
- [30] P. Shannon, et al., Cytoscape: a software environment for integrated models of biomolecular interaction networks, *Genome Res.* 13 (11) (2003) 2498–2504.
- [31] G. Bindea, et al., ClueGO: a Cytoscape plug-in to decipher functionally grouped gene ontology and pathway annotation networks, *Bioinformatics* 25 (8) (2009) 1091–1093.
- [32] D.A. Lewis, et al., Whole blood gene expression analyses in patients with single versus recurrent venous thromboembolism, *Thromb. Res.* 128 (6) (2011) 536–540.
- [33] Y. Doring, et al., Auto-antigenic protein-DNA complexes stimulate plasmacytoid dendritic cells to promote atherosclerosis, *Circulation* 125 (13) (2012) 1673–1683.
- [34] M. Steenman, et al., Identification of genomic differences among peripheral arterial beds in atherosclerotic and healthy arteries, *Sci. Rep.* 8 (1) (2018) 3940.
- [35] D. Aran, Z. Hu, A.J. Butte, xCell: digitally portraying the tissue cellular heterogeneity landscape, *Genome Biol.* 18 (1) (2017) 220.
- [36] D. Zeng, et al., IOBR: multi-omics immuno-oncology biological research to decode tumor microenvironment and signatures, *Front. Immunol.* 12 (2021) 687975.
- [37] C.T. Demisar J, A. Erjavec, C. Gorup, T. Hocevar, M. Milutinovic, M. Mozina, M. Polajnar, M. Toplak, A. Staric, M. Stajdohar, L. Umek, L. Zagar, J. Zbontar, M. Zitnik, B. Zupan, Orange: data mining toolbox in Python, *J. Mach. Learn. Res.* 14 (Aug) (2013) 2349–2353.
- [38] Z. Mallat, et al., Protective role of interleukin-10 in atherosclerosis, *Circ. Res.* 85 (8) (1999) e17–e24.
- [39] X. Han, W.A. Boisvert, Interleukin-10 protects against atherosclerosis by modulating multiple atherogenic macrophage function, *Thromb Haemost* 113 (3) (2015) 505–512.
- [40] S. Taleb, A. Tedgui, Z. Mallat, IL-17 and Th17 cells in atherosclerosis: subtle and contextual roles, *Arterioscler. Thromb. Vasc. Biol.* 35 (2) (2015) 258–264.
- [41] X. He, B. Liang, N. Gu, Th17/Treg imbalance and atherosclerosis, *Dis. Markers* 2020 (2020) 8821029.
- [42] S.J. Lee, et al., Cilostazol improves endothelial function in acute cerebral ischemia patients: a double-blind placebo controlled trial with flow-mediated dilation technique, *BMC Neurol.* 17 (1) (2017) 169.
- [43] H. Ota, et al., Cilostazol inhibits oxidative stress-induced premature senescence via upregulation of Sirt1 in human endothelial cells, *Arterioscler. Thromb. Vasc. Biol.* 28 (9) (2008) 1634–1639.
- [44] T. Hirose, S. Kurebayashi, S. Kasayama, Antiplatelet agent cilostazol potentiates adipocyte differentiation of 3T3-L1 cells, *Atherosclerosis* 158 (1) (2001) 19–22.
- [45] M.B. Elam, et al., Effect of the novel antiplatelet agent cilostazol on plasma lipoproteins in patients with intermittent claudication, *Arterioscler. Thromb. Vasc. Biol.* 18 (12) (1998) 1942–1947.
- [46] F. Sun, et al., Cilostazol inhibits plasmacytoid dendritic cell activation and antigen presentation, *J. Geriatr Cardiol* 12 (4) (2015) 388–393.
- [47] S.Y. Park, et al., Cilostazol prevents remnant lipoprotein particle-induced monocyte adhesion to endothelial cells by suppression of adhesion molecules and monocyte chemoattractant protein-1 expression via lectin-like receptor for oxidized low-density lipoprotein receptor activation, *J Pharmacol Exp Ther* 312 (3) (2005) 1241–1248.
- [48] D. Mori, et al., Cilostazol inhibits monocytic cell adhesion to vascular endothelium via upregulation of cAMP, *J Atheroscler Thromb* 14 (5) (2007) 213–218.
- [49] S.Y. Chuang, S.H. Yang, J.H. Pang, Cilostazol reduces MCP-1-induced chemotaxis and adhesion of THP-1 monocytes by inhibiting CCR2 gene expression, *Biochem. Biophys. Res. Commun.* 411 (2) (2011) 402–408.

- [50] E. Paronis, et al., Cilostazol mediates immune responses and affects angiogenesis during the acute phase of hind limb ischemia in a mouse model, *J Cardiovasc Pharmacol Ther* 25 (3) (2020) 273–285.
- [51] N.A.V. Motta, et al., Could cilostazol be beneficial in COVID-19 treatment? Thinking about phosphodiesterase-3 as a therapeutic target, *Int Immunopharmacol* 92 (2021) 107336.
- [52] W.K. Jung, et al., Cilostazol is anti-inflammatory in BV2 microglial cells by inactivating nuclear factor-kappaB and inhibiting mitogen-activated protein kinases, *Br. J. Pharmacol.* 159 (6) (2010) 1274–1285.
- [53] K.B. Min, J.Y. Min, Risk of cardiovascular mortality in relation to increased total serum IgE levels in older adults: a population-based cohort study, *Int J Environ Res Public Health* 16 (22) (2019).
- [54] Z. Xu, et al., The relationship of serum antigen-specific and total immunoglobulin E with adult cardiovascular diseases, *Int. J. Med. Sci.* 15 (11) (2018) 1098–1104.
- [55] R. Wessely, Interference by interferons: janus faces in vascular proliferative diseases, *Cardiovasc. Res.* 66 (3) (2005) 433–443.
- [56] K. Schroecksnadel, et al., Crucial role of interferon-gamma and stimulated macrophages in cardiovascular disease, *Curr. Vasc. Pharmacol.* 4 (3) (2006) 205–213.
- [57] C.LOOD, et al., Platelet transcriptional profile and protein expression in patients with systemic lupus erythematosus: up-regulation of the type I interferon system is strongly associated with vascular disease, *Blood* 116 (11) (2010) 1951–1957.
- [58] C. Mo, et al., Imbalance between T helper 17 and regulatory T cell subsets plays a significant role in the pathogenesis of systemic sclerosis, *Biomed. Pharmacother.* 108 (2018) 177–183.
- [59] J. Zhang, et al., Regulatory T cells/T-helper cell 17 functional imbalance in uraemic patients on maintenance haemodialysis: a pivotal link between microinflammation and adverse cardiovascular events, *Nephrology* 15 (1) (2010) 33–41.
- [60] C. De Ciuceis, et al., Relationship between different subpopulations of circulating CD4+ T lymphocytes and microvascular or systemic oxidative stress in humans, *Blood Press* 26 (4) (2017) 237–245.
- [61] S. Xu, et al., The role of interleukin-10 family members in cardiovascular diseases, *Int Immunopharmacol* 94 (2021) 107475.
- [62] A.M. Cates, et al., Interleukin 10 hampers endothelial cell differentiation and enhances the effects of interferon alpha on lupus endothelial cell progenitors, *Rheumatology* 54 (6) (2015) 1114–1123.
- [63] J.F. Dopheide, et al., Low IL-10/TNFalpha ratio in patients with coronary artery disease and reduced left ventricular ejection fraction with a poor prognosis after 10 years, *Inflammation* 38 (2) (2015) 911–922.
- [64] G. Caiazzo, et al., Psoriasis, cardiovascular events, and biologics: lights and shadows, *Front. Immunol.* 9 (2018) 1668.
- [65] T. Simon, et al., Circulating levels of interleukin-17 and cardiovascular outcomes in patients with acute myocardial infarction, *Eur. Heart J.* 34 (8) (2013) 570–577.
- [66] M.S. Madhur, et al., Role of interleukin 17 in inflammation, atherosclerosis, and vascular function in apolipoprotein e-deficient mice, *Arterioscler. Thromb. Vasc. Biol.* 31 (7) (2011) 1565–1572.
- [67] Y. Hirata, et al., Coronary atherosclerosis is associated with macrophage polarization in epicardial adipose tissue, *J. Am. Coll. Cardiol.* 58 (3) (2011) 248–255.
- [68] G.P. Fadini, et al., Monocyte-macrophage polarization balance in pre-diabetic individuals, *Acta Diabetol.* 50 (6) (2013) 977–982.
- [69] M. Amin, et al., Circulatory levels of C-X-C motif chemokine ligands 1, 9, and 10 are elevated in patients with ischemic stroke, *Eurasian J Med* 49 (2) (2017) 92–96.
- [70] L.P. Aristoteli, et al., The monocytic lineage specific soluble CD163 is a plasma marker of coronary atherosclerosis, *Atherosclerosis* 184 (2) (2006) 342–347.
- [71] K. Tanigaki, et al., Fcgamma receptors and ligands and cardiovascular disease, *Circ. Res.* 116 (2) (2015) 368–384.
- [72] S. Devaraj, et al., Increased expression of Fc-gamma receptors on monocytes in patients with nascent metabolic syndrome, *J. Clin. Endocrinol. Metab.* 98 (9) (2013) E1510–E1515.
- [73] J.A. Moreno, et al., The CD163-expressing macrophages recognize and internalize TWEAK: potential consequences in atherosclerosis, *Atherosclerosis* 207 (1) (2009) 103–110.
- [74] P.T. Yeh, et al., Cilostazol attenuates retinal oxidative stress and inflammation in a streptozotocin-induced diabetic animal model, *Curr. Eye Res.* 44 (3) (2019) 294–302.
- [75] S.C. Su, et al., Cilostazol inhibits hyperglucose-induced vascular smooth muscle cell dysfunction by modulating the RAGE/ERK/NF-kappaB signaling pathways, *J. Biomed. Sci.* 26 (1) (2019) 68.